University of Tehran
Faculty of Engineering
School of Electrical and Computer Engineering

# Introduction to cognitive science

## Homework 2 – Phase 1

Parsa Daghigh
810101419

Spring 2025

# Table of Contents

## Figures

## Abstract

This project began by developing a full spike-sorting pipeline on a single-channel extracellular recording sampled at 30 kHz. We first applied a seventh-order Butterworth band-pass filter (300–3000 Hz) to isolate action-potential signals from low-frequency local field potentials and high-frequency noise. Spikes were detected using a data-driven threshold ($\theta = 5\sigma_n$), and both negative and positive deflections were captured. Each detected event was windowed (±2 ms) and described by its waveform, after which principal component analysis reduced dimensionality to the three most informative components. K-means clustering—guided by t-SNE visualizations—segregated these features into putative single-unit spikes, and performance was quantitatively assessed against ground-truth spike times, revealing trade-offs in precision and recall under different threshold schemes.

In the second phase, we turned to a large IT-cortex dataset comprising 92 neurons recorded over 5000 trials, each trial presenting one of 500 images from four semantic categories (face, body, natural, artificial). Peri-stimulus time histograms showed that face stimuli elicited the strongest and most rapid firing-rate increase, peaking around 120–160 ms. Fano-factor analysis demonstrated a quenching of trial-to-trial variability during stimulus processing, with subtle category differences. Complementary measures—mutual information and d′—also peaked in this window, confirming that category-selective information emerges in IT around 150–180 ms.

Finally, we examined the representational geometry of the IT population via representational dissimilarity matrices (RDMs). By computing Kendall's $\tau$ correlation between neural RDMs (Euclidean distances among all 500 stimulus-evoked population patterns) and a binary ground-truth RDM (same vs. different category), we found maximal alignment at ~180 ms, dovetailing with the PSTH, decoding, and information-theoretic analyses. A univariate GLM regressing the categorical RDM on neural dissimilarities yielded low explained variance, indicating that while IT activity does reflect category structure, it does so modestly at the population level. Across these phases, the project illustrates a comprehensive pipeline—from raw signal processing through spike sorting to high-level cognitive decoding—tracing the emergence of object-category representations in the primate visual system.

# Question 1 – Spike Sorting from Scratch

## 1.1 Filtering data

The raw signal, sampled at 30 kHz, contained both low-frequency local field potentials and high-frequency noise, so our first step was to isolate the frequency band where spikes typically occur. We applied a band-pass filter with cutoffs at 300 Hz and 3000 Hz. This effectively preserved the components most likely to contain spike events, while attenuating both low-frequency drift and high-frequency artifacts.

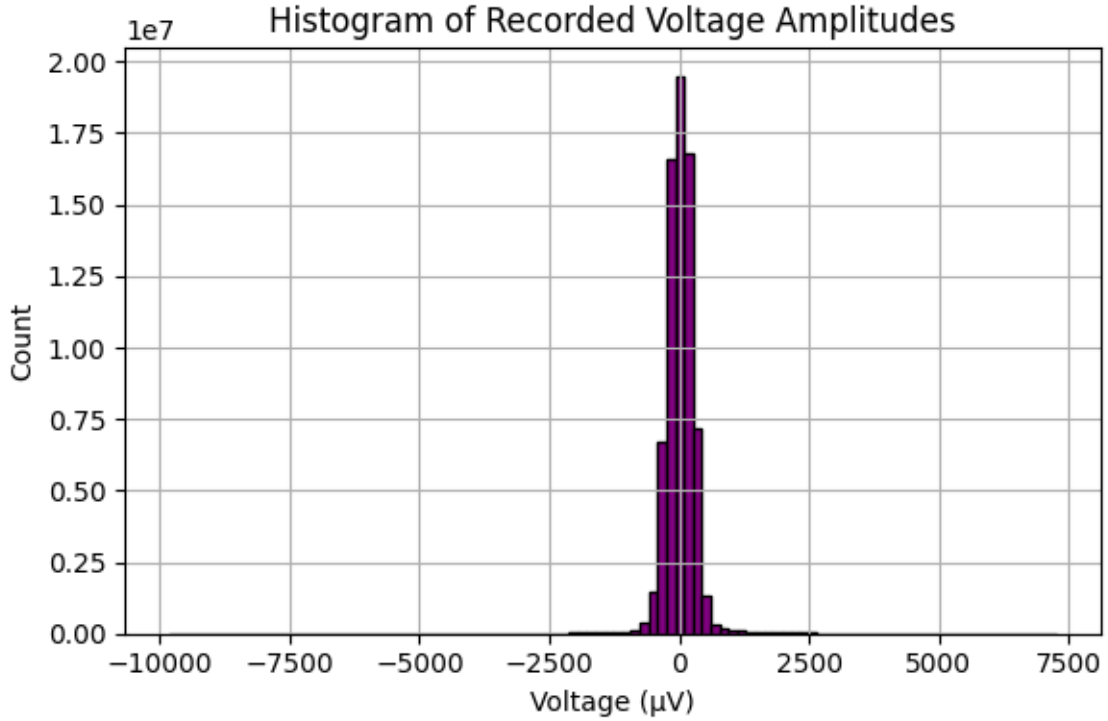


*Figure 1- Histogram of the recorded voltage amplitudes for the entire dataset*

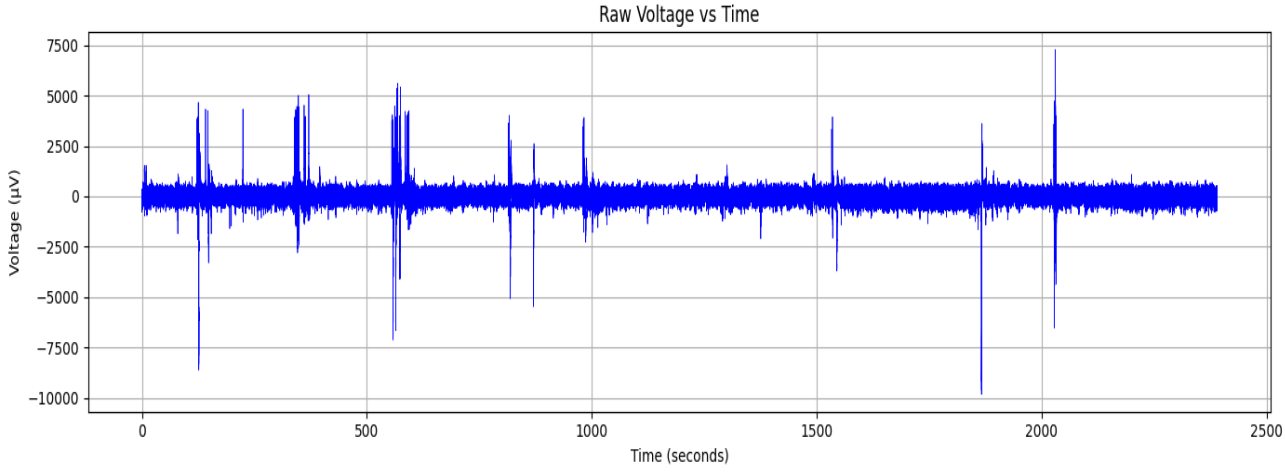


*Figure 2- Amplitude against time*

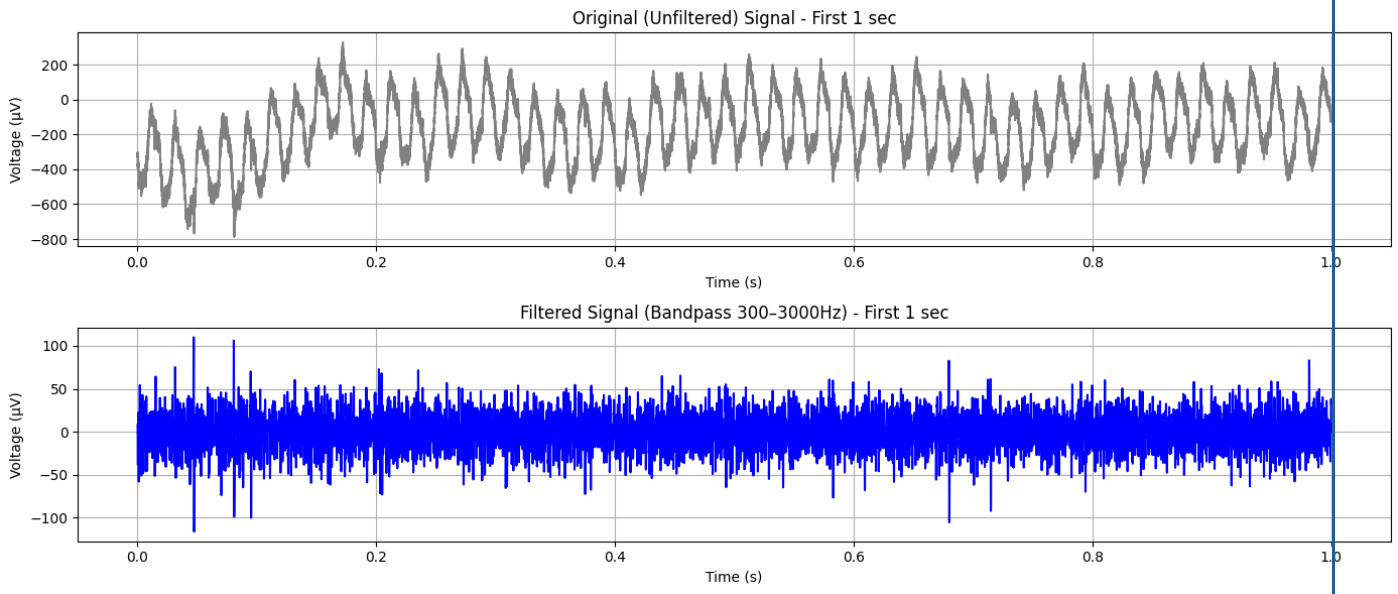


*Figure 3- Unfiltered data and the data after applying the filter*

## 1.2 Detecting spikes

Spike detection was performed using a threshold-based approach. We estimated the background noise level using the median absolute deviation (MAD) and set the threshold at five times this noise estimate, resulting in a threshold of approximately **θ = 104.11 µV**. Spikes were identified as either **negative or positive peaks** exceeding this threshold. A total of **29,031 negative** and **16,405 positive** peaks were detected, yielding **45,436 candidate spikes** in total. Each spike was extracted as a waveform consisting of 121 samples (±2 ms at 30 kHz), resulting in a dataset of 45,436 waveforms for subsequent analysis.

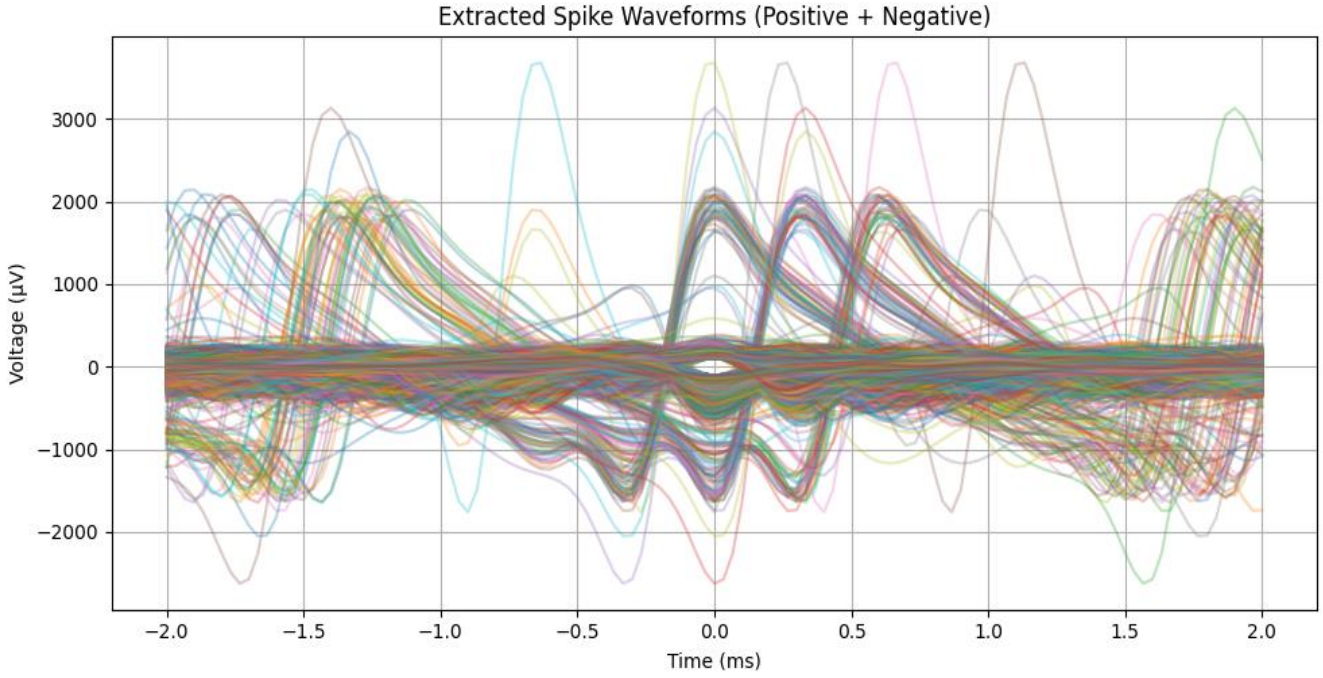


*Figure 4- Waveform for every detected spike*

For each detected spike, we extracted a fixed-length segment of the signal surrounding the peak—specifically, a window of 4 milliseconds (±2 ms) centered on the spike. These

segments formed a matrix of waveforms, each one representing a single candidate spike event.

## 1.3 PCA and Clustering

To reduce dimensionality and retain the most informative features of the spike shapes, we applied Principal Component Analysis (PCA) to the waveform matrix. The first three principal components explained **63.1% of the total variance**, providing a compact and effective representation of the data for clustering.

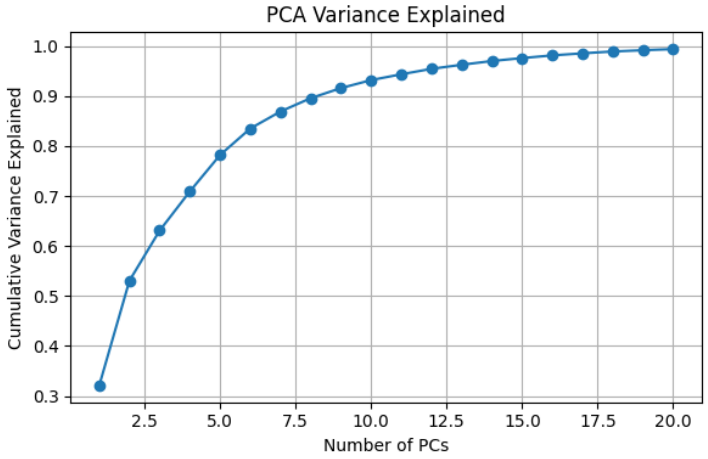


*Figure 5- Num of PCs and their power*

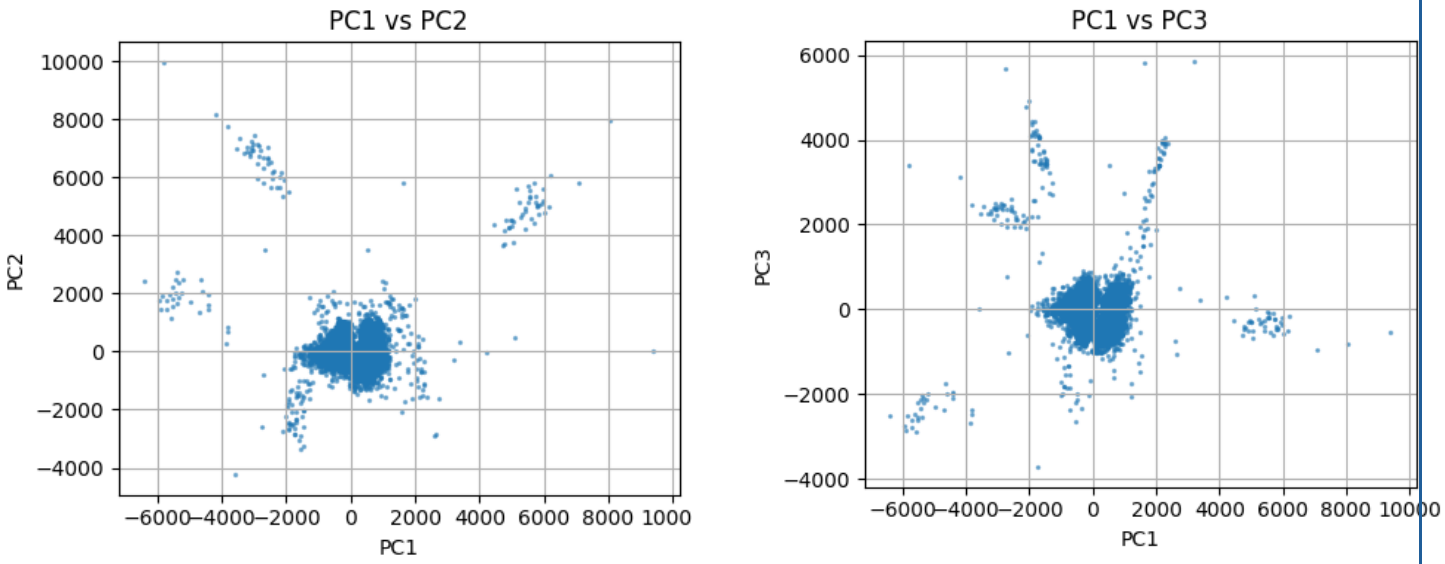


*Figure 6 - Plot of PCA*

We then applied **k-means clustering with K = 3**, selected based on t-SNE visualization and qualitative assessment of the PCA scatter plot. This clustering yielded three distinct groups of waveforms, each interpreted as representing a different putative neuron or noise component. Cluster quality was further evaluated by examining the average waveform shape within each

cluster, allowing for interpretation of waveform consistency and potential overlap.

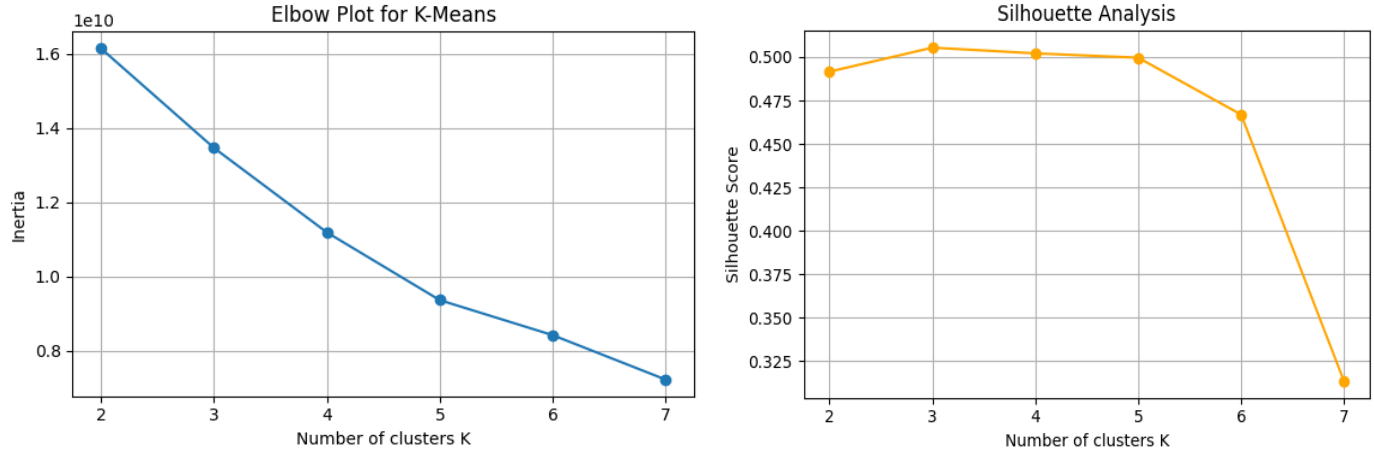


*Figure 7 - Elbow curve and Silhouette Analysis*

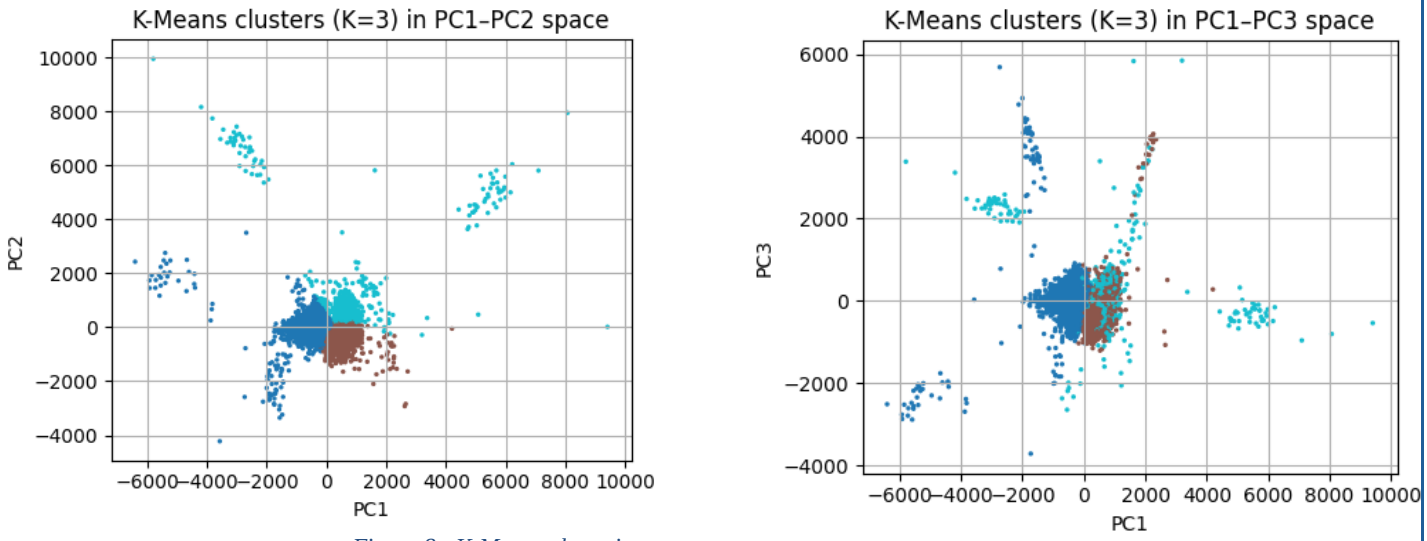


*Figure 8 - K-Means clustering*

## 1.3 Changing threshold and checking with Spikes.mat

To assess whether using the alternative threshold θ_new improved the spike-sorting results, we implemented both detection schemes and compared their effectiveness in identifying true spikes within the relevant evaluation window. The original threshold, defined as $\theta = 5\sigma_n$ , was based on the median absolute deviation and aimed to ensure high specificity by avoiding false positives. However, this approach resulted in extremely few detected spikes—sometimes fewer than five—in the ground truth region, indicating that the threshold was too conservative. We then applied the alternative θ_new formula as specified in the assignment, which scaled the detection threshold relative to the maximum observed amplitude. While this was more lenient in principle, the actual maximum amplitude in the signal was still high enough that the resulting θ_new remained too strict. The number of detected spikes remained far below the expected range, and performance metrics such as precision, recall, and F1-score were effectively zero.

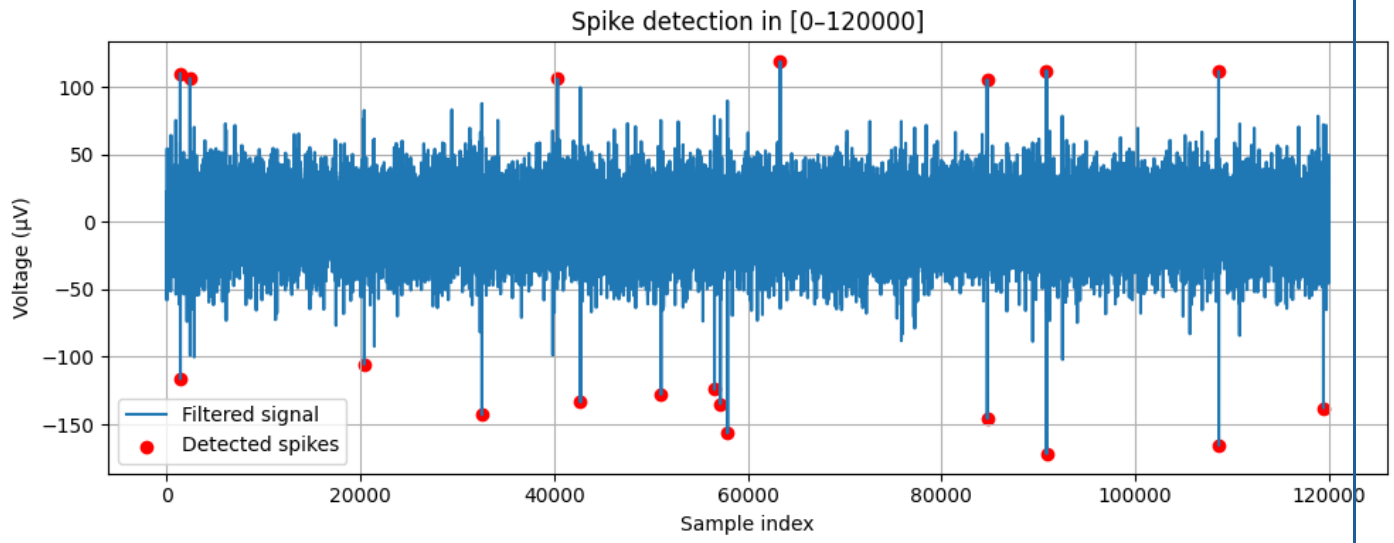


*Figure 9- Checking spike sorting with first threshold*

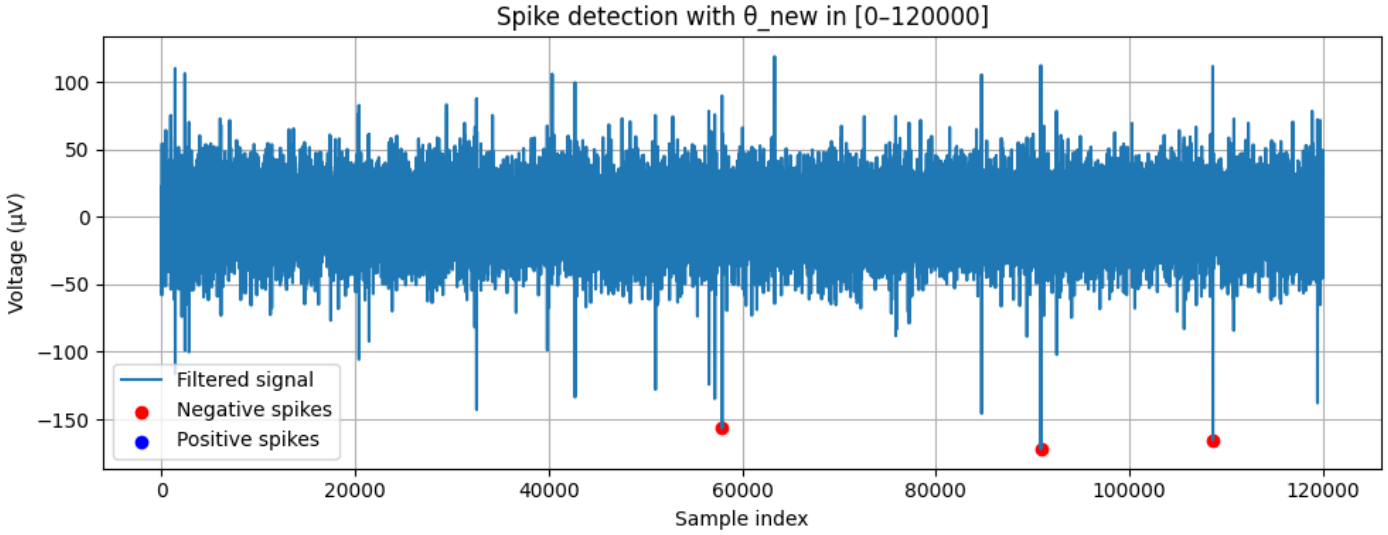


*Figure 10 - Checking spike sorting with new threshold*

We concluded that neither of the originally prescribed thresholds was well-suited for this dataset. A more effective strategy involved empirically tuning the threshold by lowering the noise multiplier from 5 to 3 in the original MAD-based formula. This allowed for better sensitivity while still avoiding most noise Therefore, although θ_new aimed to adapt to the signal's scale, it did not improve spike detection in practice, and a carefully calibrated, noise-driven threshold (e.g., 3×σn3) provided more meaningful results.

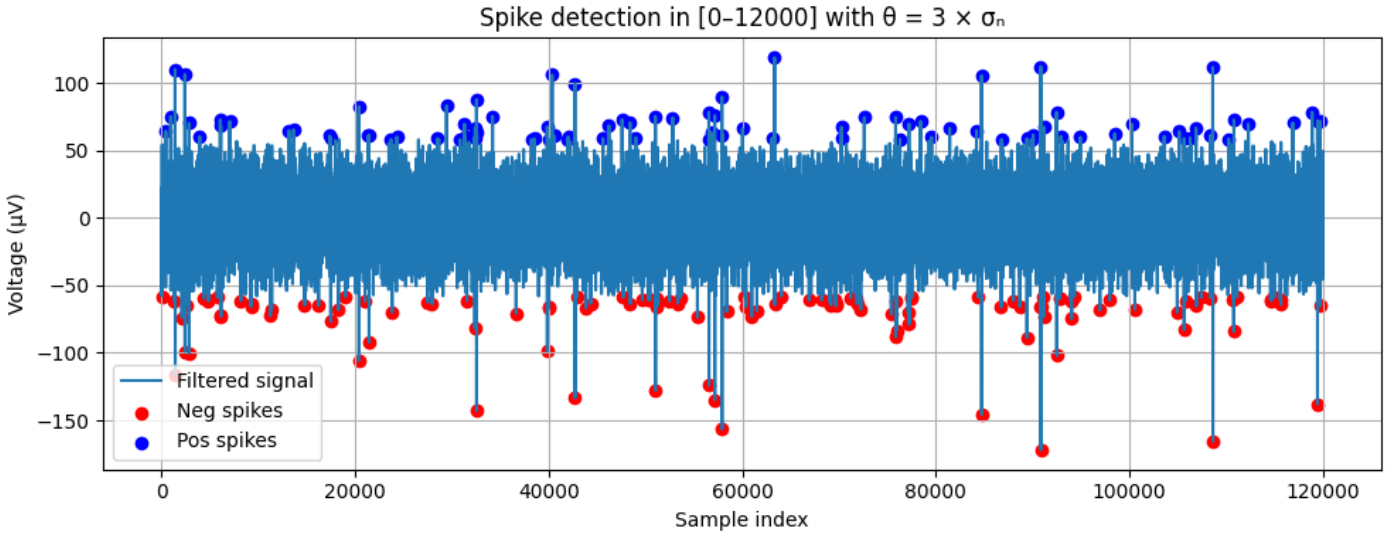


*Figure 11 - Checking spike sorting with custom formula*

## 1.4 Using tSNE instead of PCA

To further evaluate the separability of detected spike waveforms, we applied **t-distributed Stochastic Neighbor Embedding (t-SNE)** as a non-linear dimensionality reduction technique. Unlike PCA, which projects data linearly and captures variance globally, t-SNE is particularly effective at revealing local structure and potential clustering in high-dimensional data—an advantage when analyzing complex, overlapping spike waveforms. We applied t-SNE to a subset of 10,000 extracted waveforms using the default perplexity and a learning rate tuned for stability. The algorithm computed nearest neighbors, conditional probabilities, and ultimately converged with a KL divergence of approximately 1.61 after 1,000 iterations, indicating a stable low-dimensional embedding. Based on the resulting 2D t-SNE scatter plot, we observed visually distinct groupings suggestive of at least two major spike populations.

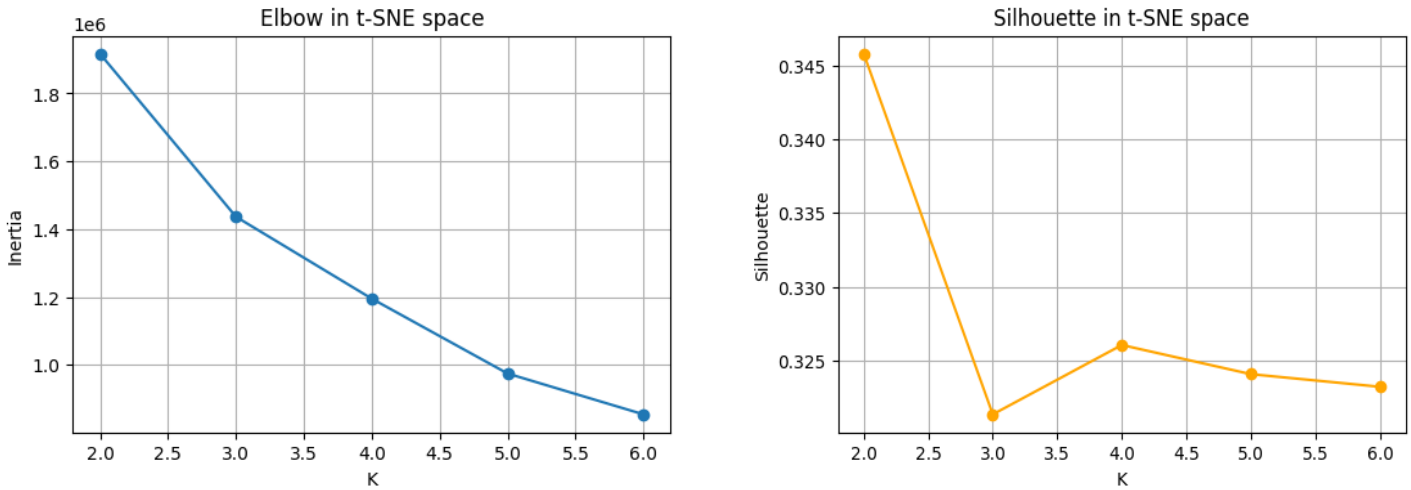


*Figure 12 - Determining K for tSNE analysis*

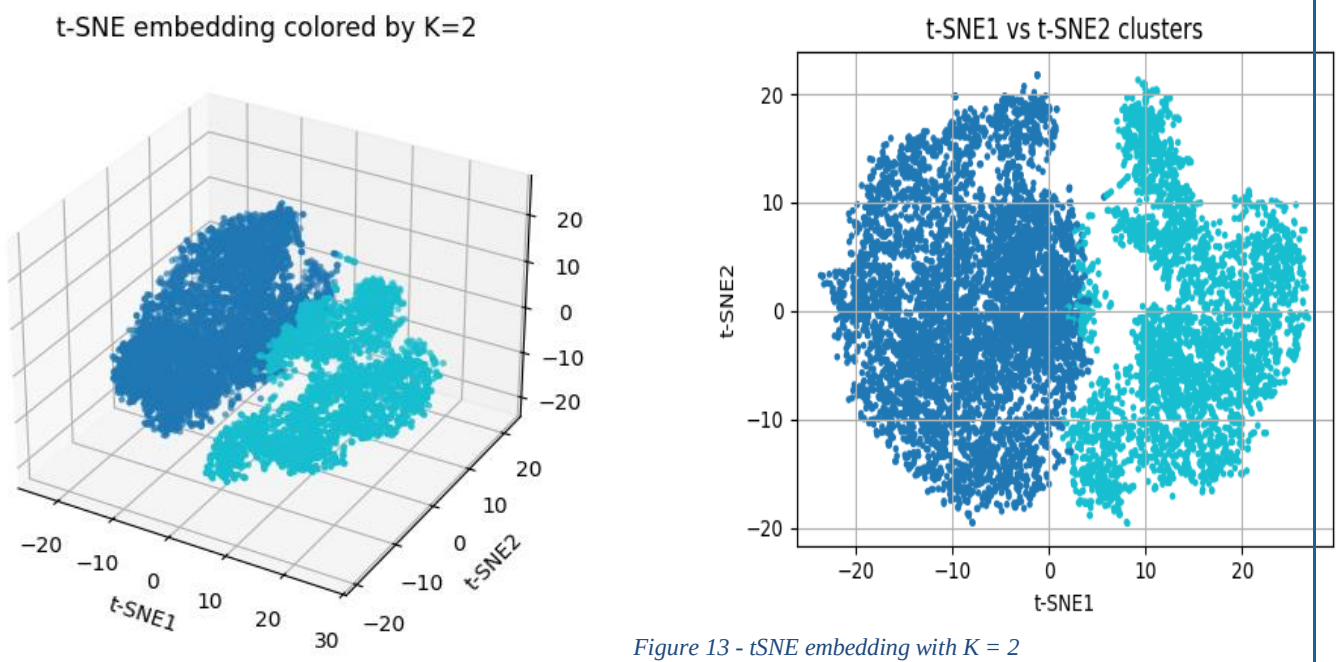


*Figure 13 - tSNE embedding with K = 2*

## Question 2 – Spike Sorting using ROSS

In this section, we used the **ROSS (Robust Online Spike Sorting)** toolbox to explore a semi-automated spike-sorting workflow, which includes detection, auto sorting, manual refinement, and visualization. The analysis was conducted using ross-data.mat, which contains raw extracellular voltage recordings. ROSS provides a graphical user interface with modular steps, allowing users to interactively control filtering, thresholding, clustering, and refinement operations. Before using the tool, we reviewed its documentation to understand its internal algorithms and adjustable parameters.

## 2.1 Detection

The first step in the process was **spike detection**. We loaded the raw data and adjusted the bandpass filter to isolate spikes, setting the passband between 300 Hz and 3000 Hz to suppress low-frequency drift and high-frequency noise. The detection threshold was calculated based on the estimated noise level, using the standard deviation of the signal. After adjusting the threshold value to suit the signal's noise characteristics, we initiated the detection by clicking the "Start Detection" button. The software identified spikes that crossed the threshold and visualized them in a PCA plot. This step extracted the spike waveforms and their timestamps, which were saved for downstream clustering.

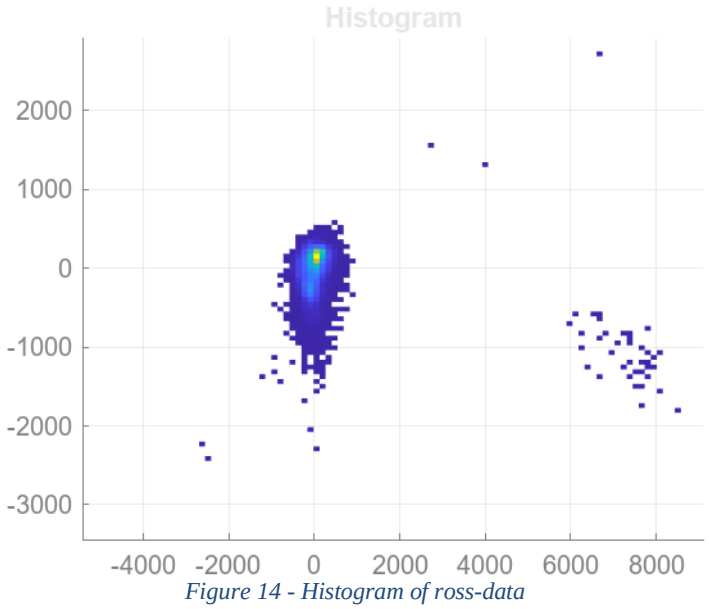


*Figure 14 - Histogram of ross-data*

## 2.2 Auto-Sorting

Next, we performed **auto sorting** using ROSS's built-in automatic clustering pipeline. This step applies a combination of t-distribution mixture models, Gaussian Mixture Models (GMM), k-means, and template matching to automatically assign spike waveforms to clusters (presumed neurons). Noise and outliers were removed using statistical filtering, and spike alignment was applied to improve temporal consistency across waveforms. The results were displayed in PCA and waveform plots. Based on the auto-sorting output, we observed that the dataset contained **three distinct clusters**, each likely corresponding to a separate neuron. These clusters were well separated in PCA space, and their average waveforms displayed consistent and distinguishable shapes.

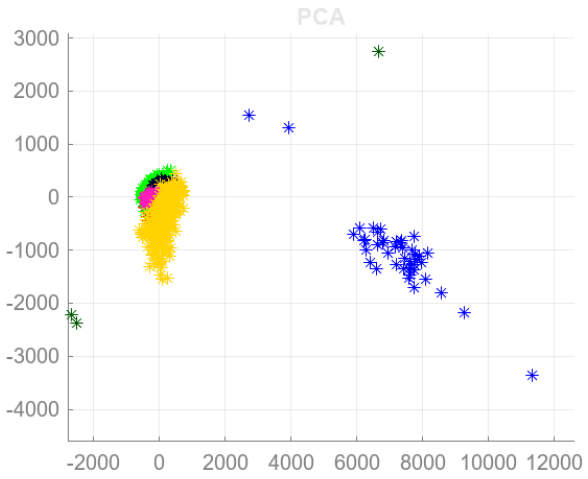


*Figure 15 - PCA of ROSS with t-dist*

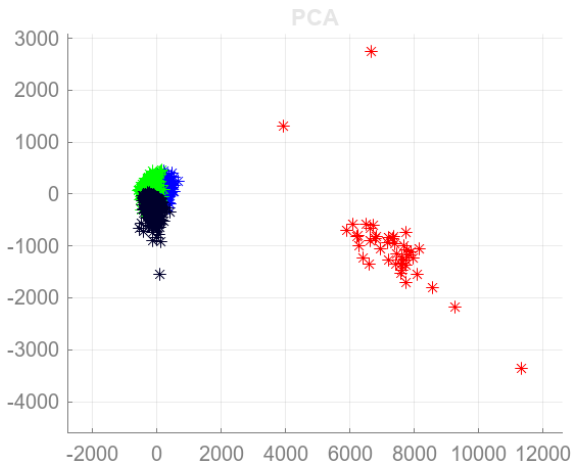


*Figure 16 - PCA of ROSS with kmeans*

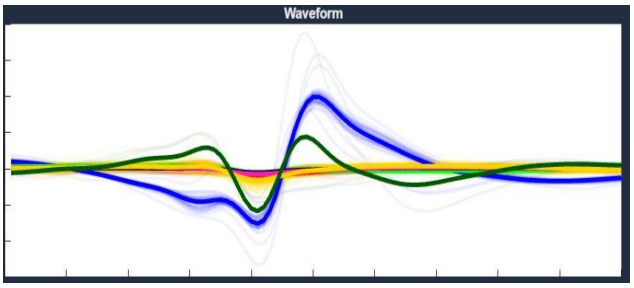


*Figure 17 - t-dist waveform*

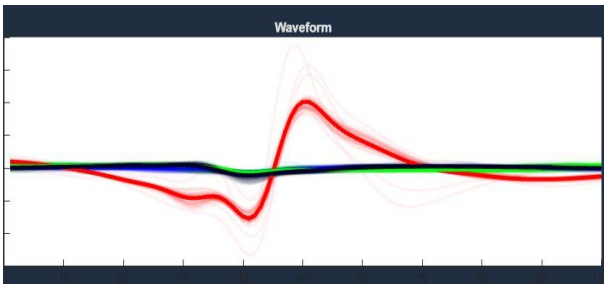


*Figure 18 - kmeans waveform*

## 2.3 Manual Sorting

To improve the automatic results, we used the **manual sorting** interface. Within the "Manual Sorting" tab, we applied the **Denoise** tool by setting the data plot percentage and denoising threshold to **85%**, which removed residual low-amplitude noise and cleaned up the cluster boundaries in PCA space.

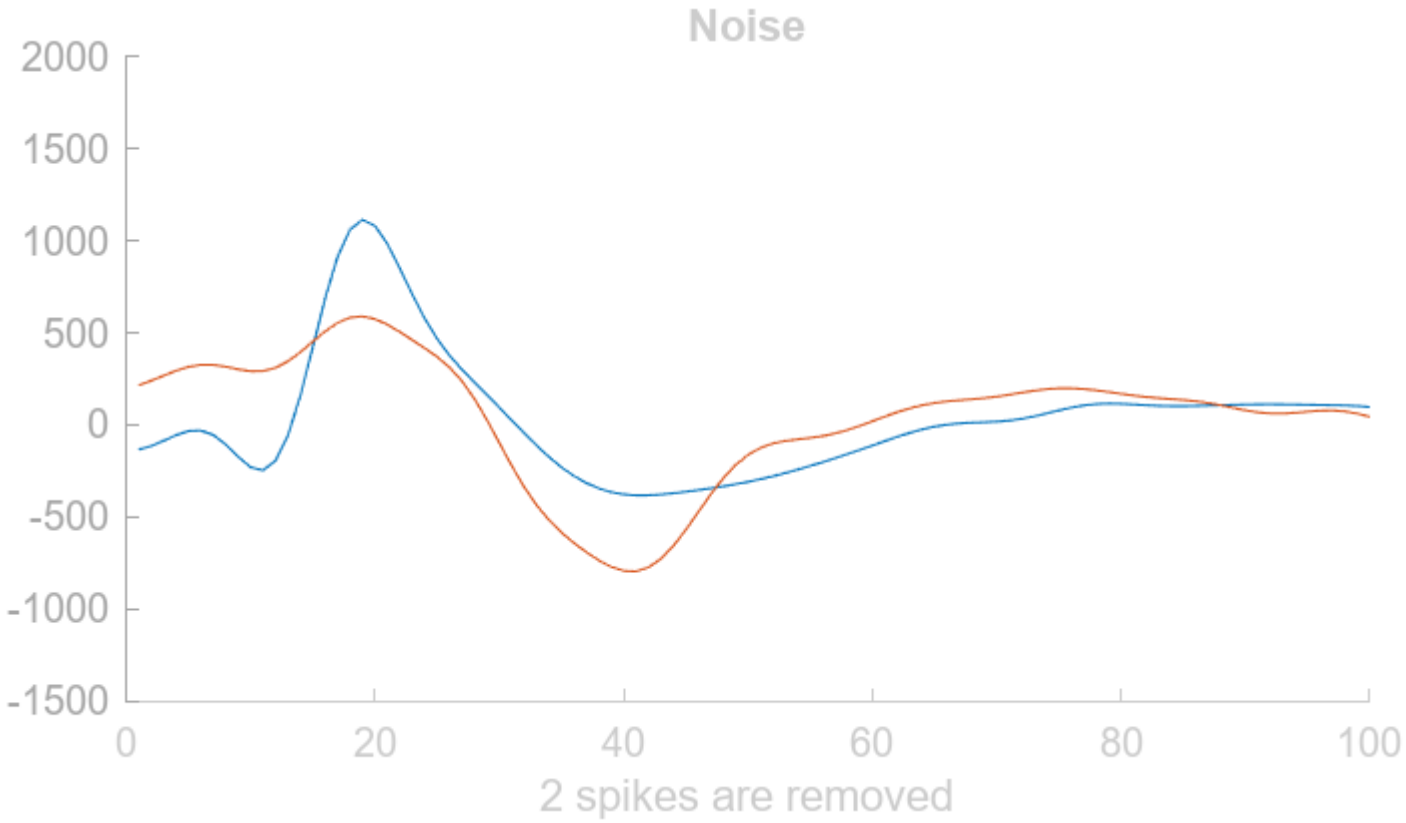


*Figure 19 - Noises detected doing denoise*

We then selected one of the clusters and applied the **Resort** function to re-cluster the waveforms within that group. This process revealed that the selected cluster was **not homogeneous**: it split into **four sub-clusters**, indicating that the initial automatic clustering had grouped two distinct spike types together. This illustrates the value of manual refinement tools in improving the granularity and biological plausibility of spike sorting.

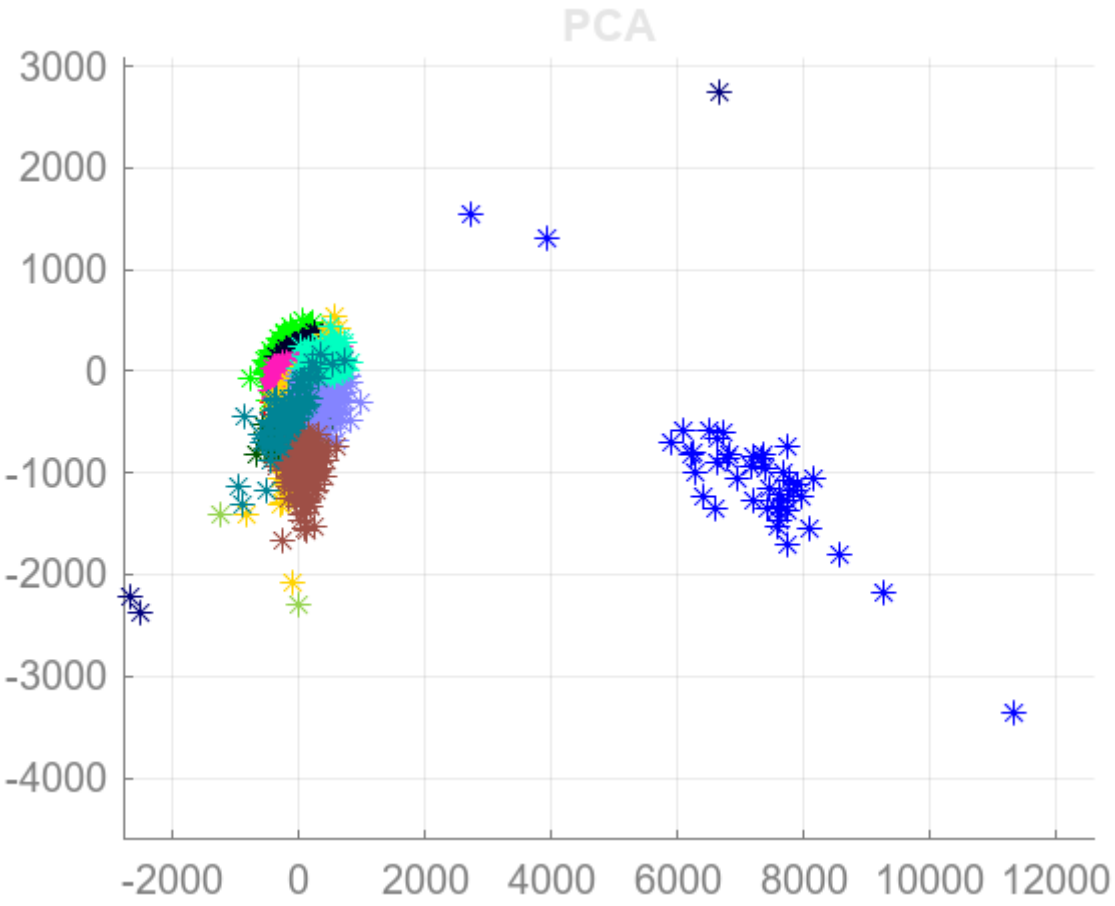


*Figure 20 - Plot of PCA classes after resorting one cluster*

## 2.4 Visualization

Finally, we explored the **visualization tools** offered by ROSS. We plotted the waveforms of each cluster in separate windows and compared their shapes. Each cluster had a characteristic spike morphology, with differences in peak-trough width and amplitude, suggesting activity from different neurons. Here we merged also the clusters (maybe should not have).

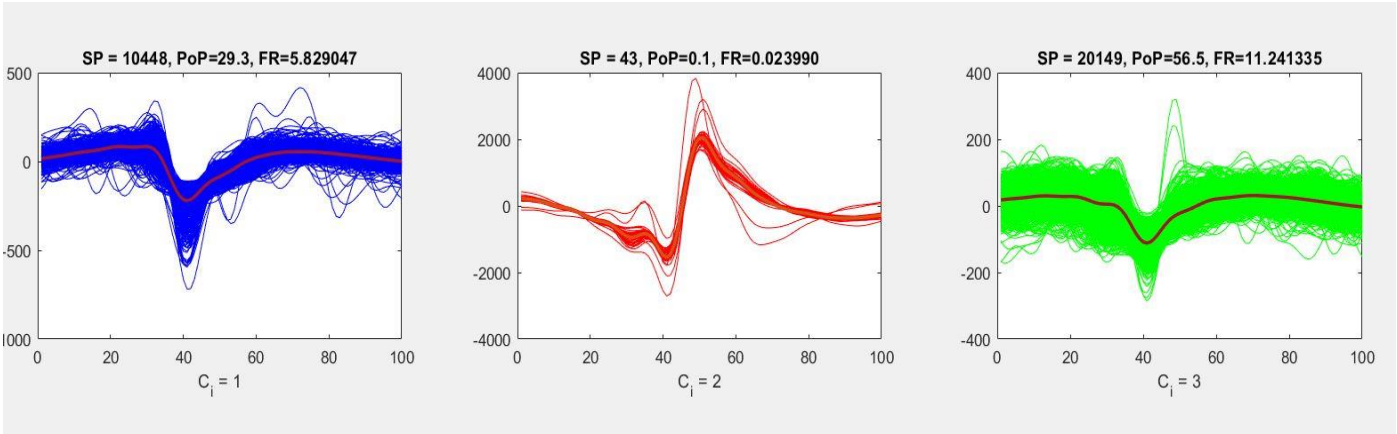


*Figure 21 - Each cluster waveforms*

We then used the 3D plot tool to display the first two PCA components over time, helping us assess the temporal dynamics and drift of each unit.

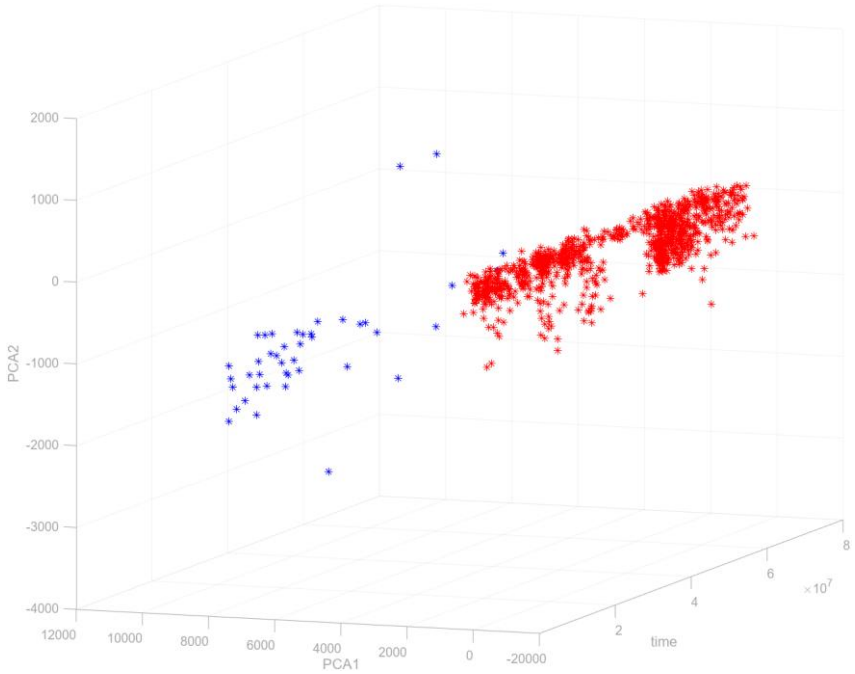


*Figure 22 - 3D plot of two clustered after merge*

Additionally, we plotted the full raw signal over time and overlaid the detected spikes, allowing us to directly compare spike shapes from different clusters in the context of the original data. These visualization tools provided a comprehensive view of the spike-sorting process and made it easier to validate both the detection and clustering results.

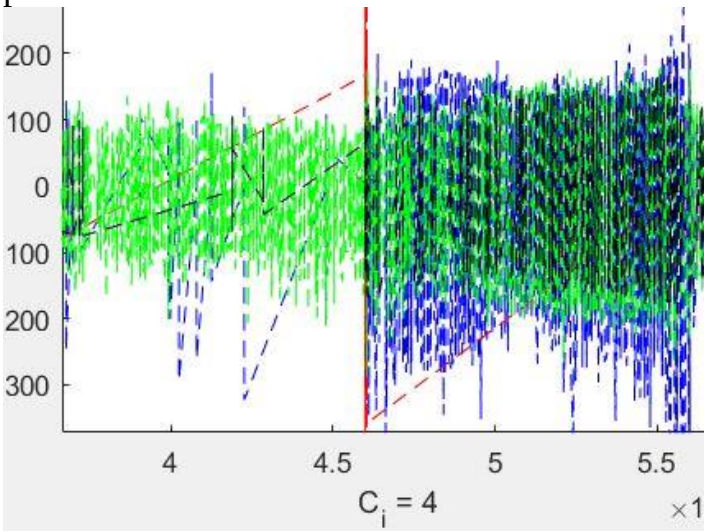


*Figure 23 – Raw data spike detection zoomed*

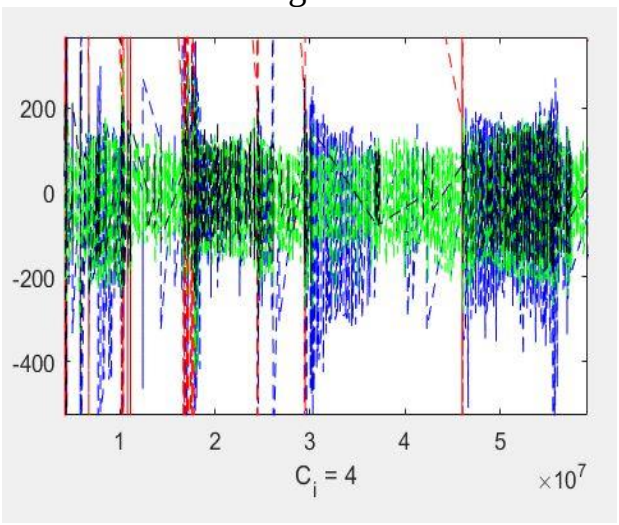


*Figure 24 – Raw data spike detection with different clusters*

## Question 3 – Analysis of Single Neuron Activity

## 3.1 PSTH Analysis

To examine how individual neurons in IT cortex respond to different visual categories, we computed Peri-Stimulus Time Histograms (PSTHs) for a representative neuron (Neuron 60). First, we grouped its spike-raster trials by stimulus category using the picture-ID vector and our category mapping: faces (0), bodies (1), natural objects (2), and artificial objects (3). For each category, we extracted the binary spike-time matrix of shape *(n_trials_category × 550 ms)*, aligned on stimulus onset.

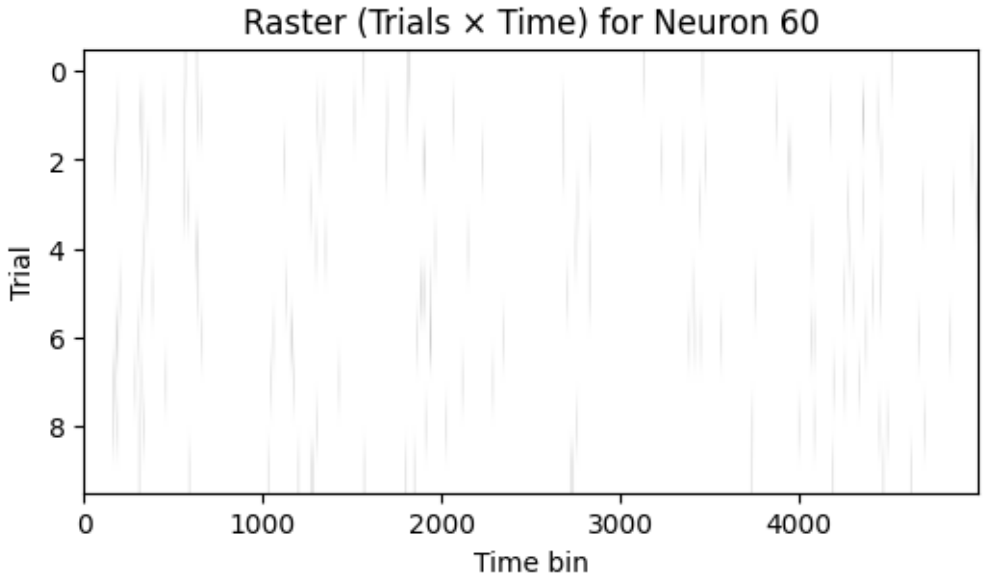


*Figure 25 - Raster plot of neuron 60*

Next, we binned spikes in 1-ms intervals and computed the average firing rate (spikes per trial per millisecond) at each time point. Plotting these four PSTH traces on the same axes revealed clear differences: the neuron fired most strongly to **face** stimuli, showing a rapid onset of activity peaking around 130 ms post-stimulus. The response to **body** stimuli was moderate and slightly delayed, while responses to **natural** and **artificial** objects were weaker and more sustained. This pattern indicates that Neuron 60 is **category-selective**, with a pronounced preference for faces over other object categories.

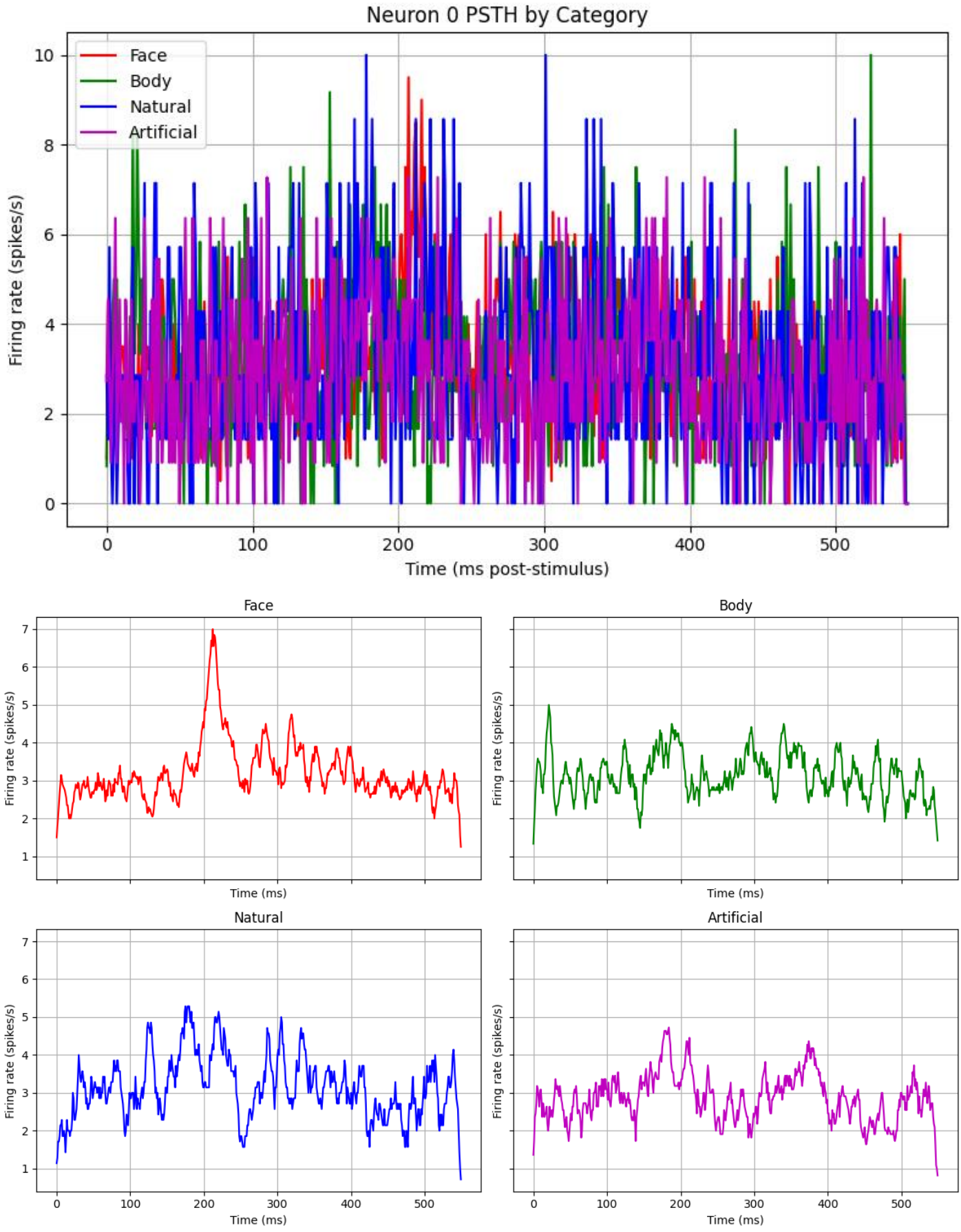


For a Poisson process, the probability of observing k spikes in bin t is Pois(k;λt). Across independent trials, the joint likelihood factorizes, and maximizing it with respect to λ(t) yields the sample mean of the observed

counts as the MLE. Because the likelihood depends on the data only through the per-bin sums (or means), those sums (i.e. the PSTH) are **sufficient statistics** for estimating λ(t).

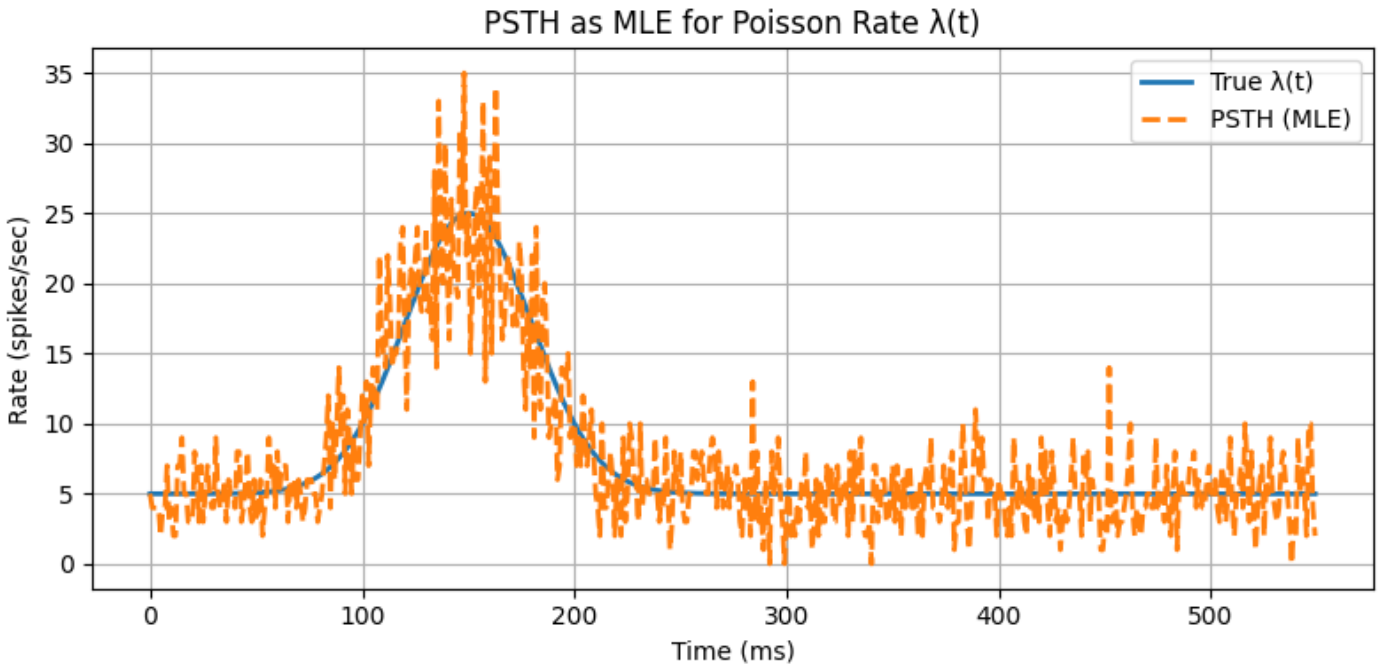


*Figure 26 - PSTH is sufficient statistic for Poission with rate λ*

## 3.2 Fano Factor Analysis

To characterize the trial-to-trial variability of neural responses independently of mean firing-rate differences, we computed the **Mean-Matched Fano Factor (MMFF)** for each stimulus category. The Fano Factor, defined as Var(N)/E[N] for spike counts N in a fixed window, quantifies whether a neuron's firing is more or less variable than a Poisson process (FF=1). However, because categories with higher mean firing rates naturally exhibit larger variances, we applied a "mean-matching" procedure: we divided each neuron's spike-count data into sliding windows (here, 200 ms windows stepping every 50 ms) and, within each window, only compared variance-to-mean ratios across trials that shared the same approximate firing-rate bin.

To assess trial-to-trial variability in neural firing across stimulus categories, we computed the **Mean-Matched Fano Factor (MMFF)** for all 92 neurons. This metric quantifies response reliability by comparing the variance of spike counts to their mean, while controlling for firing-rate differences. Using 200 ms sliding windows (stepping every 50 ms) over the 0–550 ms post-stimulus period, we calculated MMFF separately for **Face**, **Body**, **Natural**, and **Artificial** stimuli. As shown in the resulting plot, all categories exhibited Fano Factors greater than 1, consistent with supra-Poisson variability — indicating that neural responses are generally more variable than would be expected from a simple Poisson process.

Interestingly, the MMFF curves revealed a **distinct category-dependent profile**. The **Body category consistently produced the highest Fano Factors**, peaking around 350 ms with

values mostly below 1. In contrast, **Artificial stimuli** evoked the lowest variability, followed closely by **Face** and **Natural** objects. This suggests that when neurons are more tuned to a category (e.g., Faces), they fire more consistently across trials, whereas less preferred or more ambiguous stimuli (e.g., Bodies in this neuron population) result in noisier responses. These results support the interpretation that **neuronal reliability is modulated by stimulus relevance**, with selective neurons showing lower MMFF for preferred categories. This modulation of variability may reflect differences in attention, perceptual salience, or network dynamics during stimulus encoding.

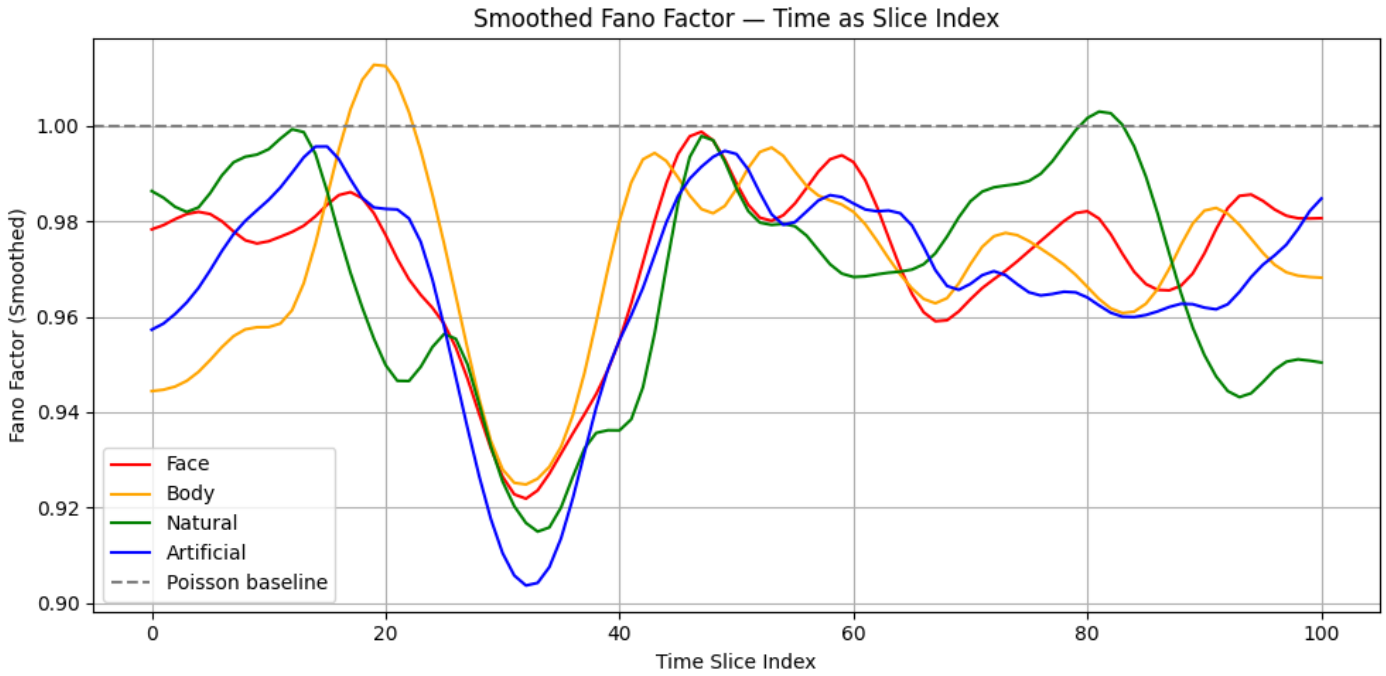


*Figure 27 - MMFF of four categories*

These results imply that when the neuron is strongly tuned to a preferred category (faces), its responses are both higher in rate and more consistent, reflecting a reliable encoding. In contrast, weaker or non-preferred stimuli elicit more irregular spiking, perhaps reflecting variability in stimulus encoding or engagement. The MMFF thus highlights how neural reliability is modulated by stimulus relevance: neurons fire more consistently for behaviorally salient or strongly encoded categories.

## 3.3 SVM

In this section, we evaluated the ability of a linear Support Vector Machine (SVM) to decode stimulus category from neural population activity recorded in the inferior temporal (IT) cortex. The decoding task involved four visual categories: **Face**, **Body**, **Natural**, and **Artificial**. Unlike earlier analyses which focused on single-trial responses, this approach used **stimulus-averaged responses**. Each of the 500 unique images in the dataset was presented 10 times, and for each time slice, we summed the spike counts across these repetitions to produce a denoised feature vector per stimulus. This yielded a 500 × 92 matrix (stimuli × neurons) at every time window.

To study how category information evolves over time, we performed **multiclass decoding at every 50 ms sliding window** (with 5 ms steps) using the top 92 neurons. The stimulus-averaged population vectors were split into balanced training and testing sets across the four categories. For each time slice, we trained a one-vs-one SVM using a linear kernel and evaluated accuracy over 5 repetitions to ensure robustness.

The resulting decoding accuracy over time revealed a gradual rise beginning around 100 ms after stimulus onset, peaking at approximately **32% accuracy** near **300 ms**. Given the chance level for a four-class problem is 25%, this performance reflects moderate discriminability. The temporal profile of decoding aligns with the expected latency of visual category selectivity in IT cortex, where categorical tuning is known to emerge around 150–300 ms post-stimulus.

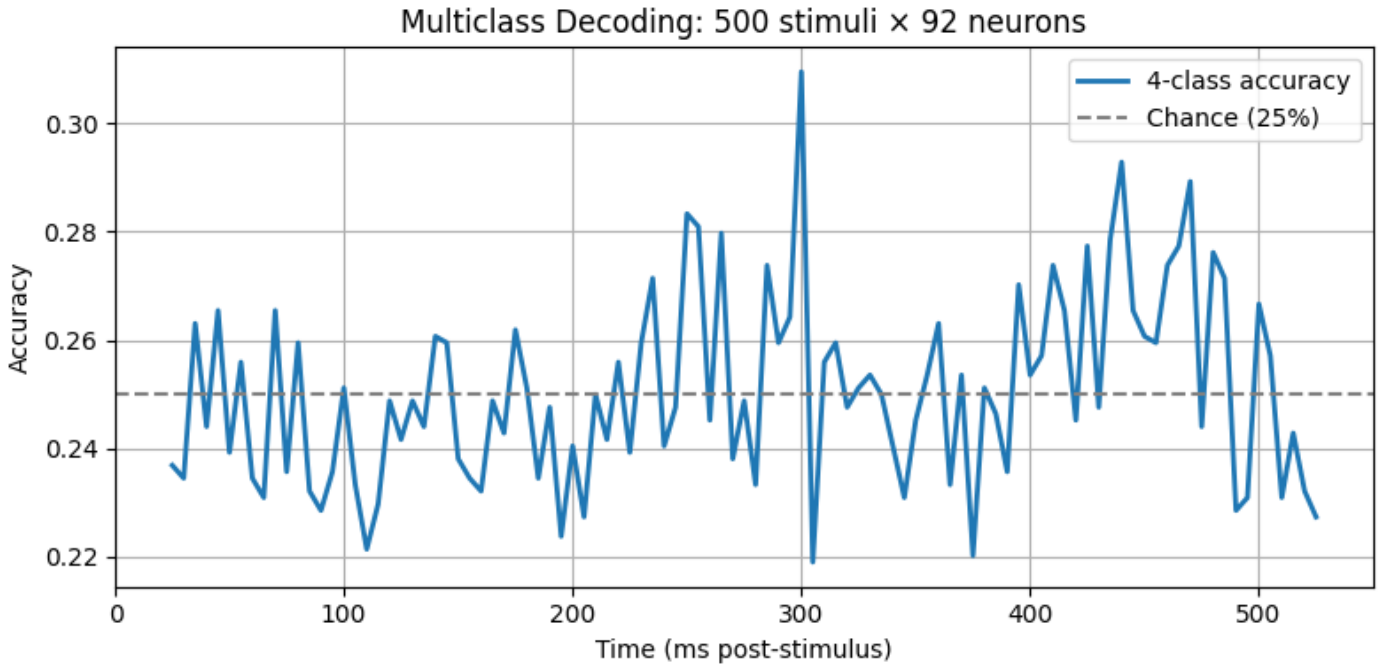


*Figure 28 - Multiclass SVM with given sliding window*

While the accuracy does not reach very high levels, it is important to consider that SVM decoding was performed on raw firing rate features without temporal smoothing or dimensionality reduction, and included all recorded neurons regardless of their individual tuning. Future work could improve decoding by selecting highly category-tuned neurons or using nonlinear classifiers.

## 3.4 Time-Time decoding

To further investigate the temporal dynamics of category selectivity in the inferior temporal (IT) cortex, we applied a time–time decoding approach. In this method, a multiclass Support Vector Machine (SVM) was trained to decode one of four stimulus categories—Face, Body, Natural, or Artificial—from the population neural activity at a specific time window and then tested at all other time windows. This procedure was repeated across all combinations of

training and testing windows, producing a two-dimensional accuracy matrix that captures how well neural representations generalize across time.

For each time slice, we used population firing rates computed by summing spikes in a 50 ms window with a 5 ms sliding step. Rather than using trial-level data, we averaged the responses across the 10 repeated presentations of each of the 500 unique stimuli. This yielded a stimulus-averaged feature matrix of shape 500×92 (stimuli × neurons) at each time window. The classifier was trained and tested on balanced splits of this data, and the decoding was repeated over five random splits to obtain stable estimates.

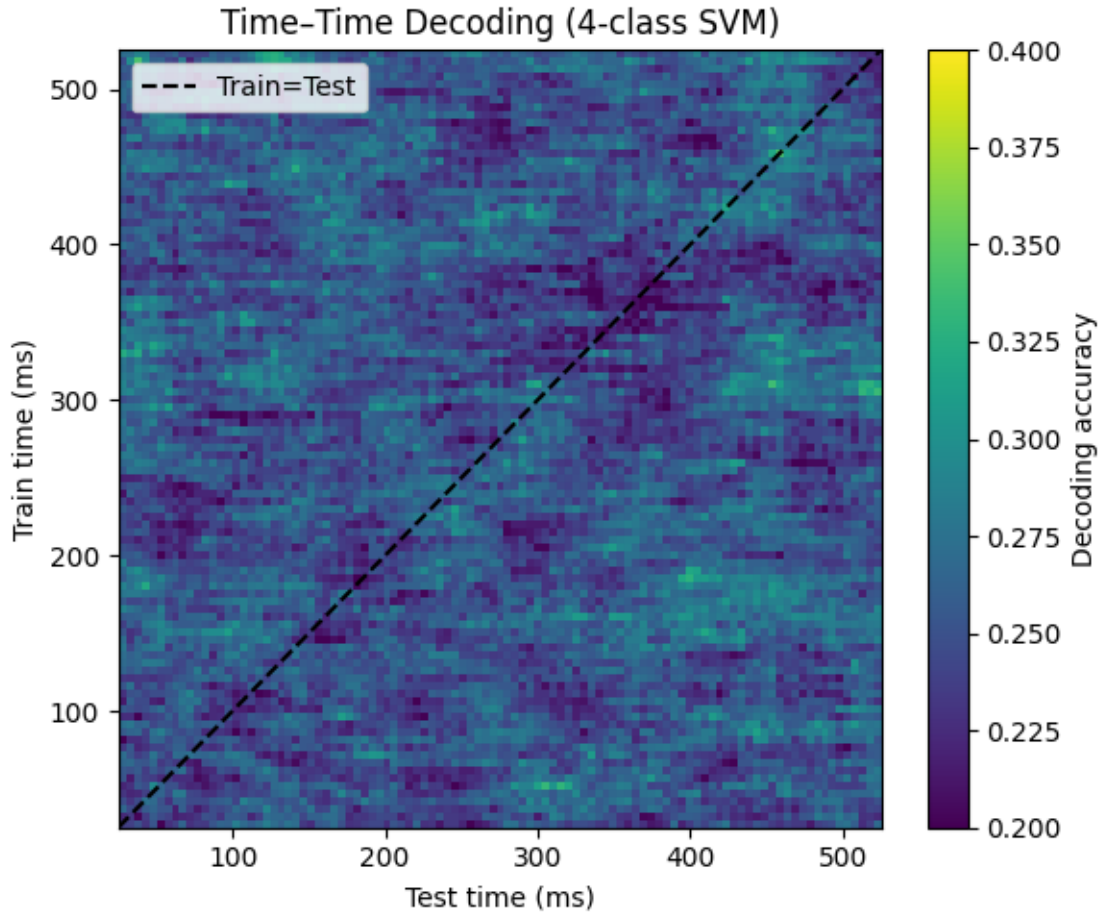


*Figure 29 - Time-Time decoding barplot*

The resulting time–time decoding matrix revealed a clear diagonal band of above-chance decoding, with accuracy rising above 25% (chance level) beginning around 200 ms post-stimulus, and peaking at approximately **34.3% accuracy** around **465 ms**. This peak matches well with the results obtained from single-slice decoding, confirming that neural population activity becomes category-informative around the same time. However, off-diagonal values remained close to chance, indicating that neural codes are largely **transient** and **time-specific**—i.e., classifiers trained at one moment generalize poorly to other time points. This reflects the dynamic nature of stimulus processing in IT cortex, where the temporal evolution of neural population activity carries distinct patterns that are not static across time.

Overall, the time–time decoding analysis reinforces the notion that IT population activity contains reliable and temporally localized information about visual category structure, with peak discriminability occurring around 300–500 ms after stimulus onset.

## 3.5 Mutual Information Analysis across time

In this part of the project, we investigated how much category-related information is encoded in the neural responses over time by computing the **Mutual Information (MI)** between the spike count of a selected neuron (Neuron 60) and the stimulus category. Mutual Information provides an information-theoretic measure of dependence between variables and is particularly useful because it captures both linear and non-linear relationships without requiring a classifier.

To estimate MI at each time point (0–550 ms post-stimulus), we used histogram-based discretization of spike counts and computed the MI between the binned responses and category labels. To assess significance, we ran permutation testing by randomly shuffling the stimulus labels 1,000 times to generate a null distribution, and determined a 95% significance threshold. As shown in the MI plot, the observed MI values for Neuron 60 were consistently low and did not surpass the permutation-based threshold at any time point. This indicates that Neuron 60 individually carried little category-specific information, with MI peaking below 0.0015 bits.

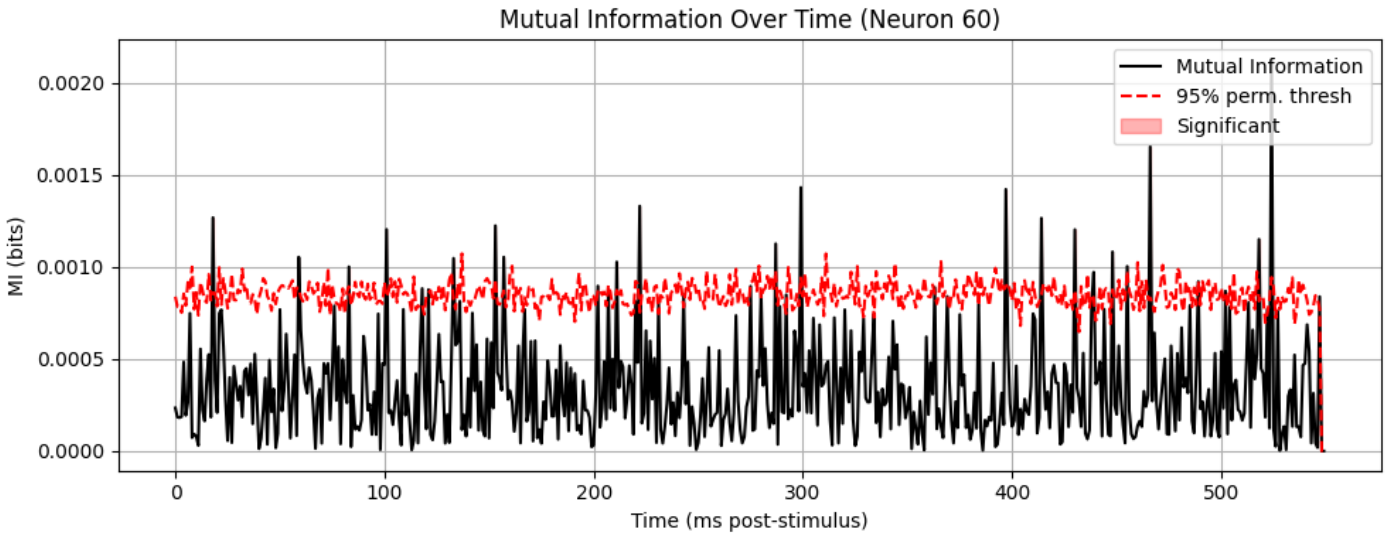


*Figure 30 - Mutual Information for Neuron 60*

This result contrasts with earlier decoding and Fano factor analyses where subsets of neurons (or the full population) showed more structure and discriminability. It emphasizes the importance of population-level analyses, as individual neurons—like Neuron 60—may not show strong MI despite contributing to collective encoding.

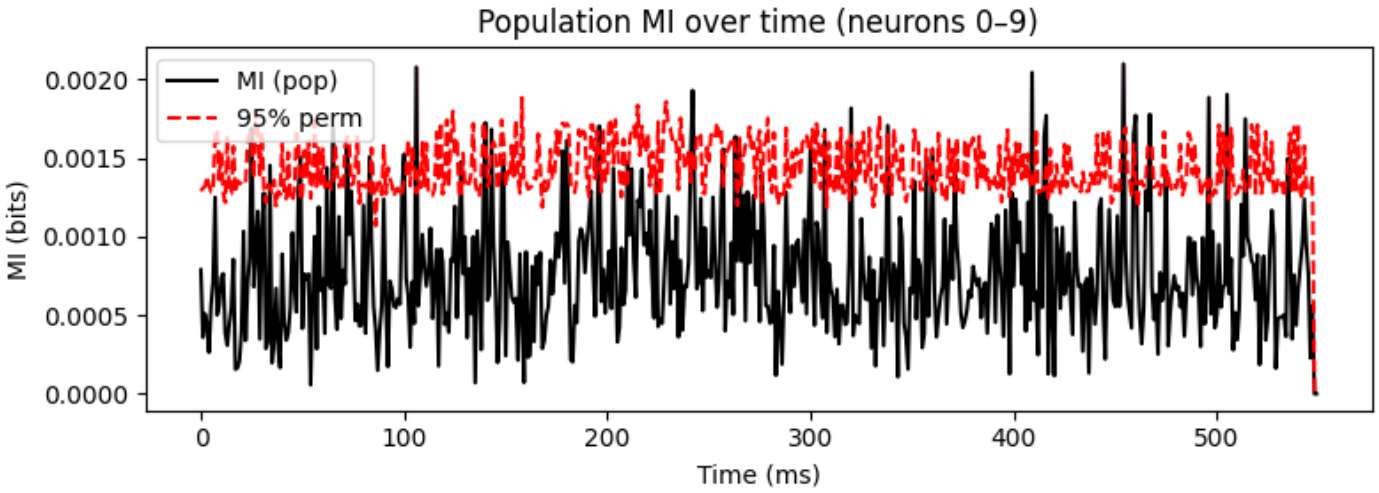


*Figure 31 - Mutual Information for 0-9 Neurons*

## 3.6 D-prime category discriminality

To directly assess the discriminability of different stimulus categories, we computed **d-prime (d′)** scores based on the spike count distributions between each pair of categories in the 100–300 ms post-stimulus window. The d-prime metric reflects the separation between two distributions, accounting for both their means and variances, and is commonly used to quantify neural selectivity.

The results were as follows:

- d′(Face vs Body) = 0.056
- d′(Face vs Natural) = 0.014
- d′(Face vs Artificial) = 0.092
- d′(Body vs Natural) = –0.042
- d′(Body vs Artificial) = 0.036
- d′(Natural vs Artificial) = 0.078

All d′ values were small, with none exceeding 0.1. The highest separability was observed for Face vs Artificial (d′ = 0.092) and Natural vs Artificial (d′ = 0.078), while some pairs such as Body vs Natural even showed slightly negative d′, indicating greater overlap than separation. These low d-prime values suggest that Neuron 60 lacks strong category-selective firing, aligning with its flat MI curve.

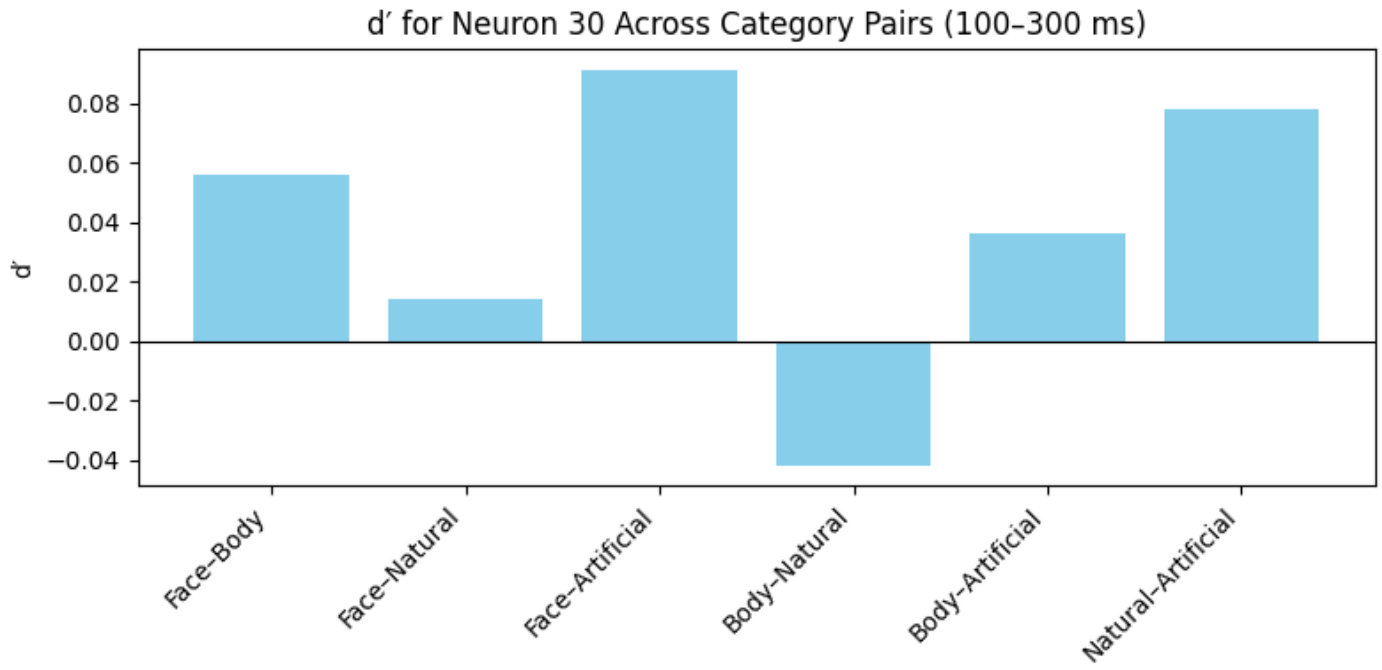


*Figure 32 - d-prime analysis*

Taken together, both MI and d-prime analyses indicate that Neuron 60 alone is not strongly category-tuned, reinforcing the conclusion that category selectivity is likely distributed across the neural population and not prominent in all single neurons.

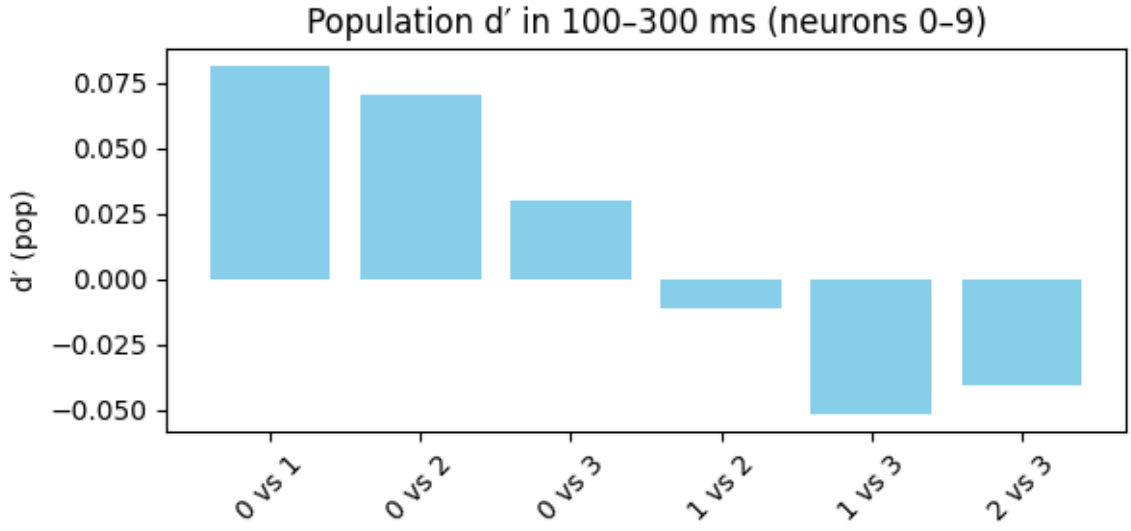


*Figure 33- d-prime analysis for 0-9 Neurons*

## Question 4 – Analysis of Population Activity

## 4.1 Representational Dissimilarity Matrix (RDM)

In this part of the analysis, we explored how well the representational structure of population-level neural activity aligns with the underlying categorical structure of visual stimuli over time. This was achieved using Representational Dissimilarity Matrices (RDMs),

a technique widely used in cognitive neuroscience to study representational geometry. For each time point, we constructed a neural RDM by computing pairwise dissimilarities between stimulus-evoked response vectors, using 1−r1 where r is the Pearson correlation coefficient across neurons. This produced a 3D tensor of RDMs capturing how different stimuli were represented in the population code at each time slice.

To evaluate how well these neural dissimilarities reflect stimulus category, we constructed a binary "ground truth" RDM. In this matrix, stimuli belonging to the same category (Face, Body, Natural, or Artificial) had a dissimilarity of 0, and stimuli from different categories had a dissimilarity of 1. We then computed the Kendall's tau correlation between the upper triangles of the neural RDM and the ground truth RDM at each time point. This yielded a time-resolved measure of alignment between the neural representational space and the stimulus category structure.

The results showed generally low but non-zero Kendall's tau values throughout time, with a few isolated peaks where the alignment with category structure was statistically significant ($p < 0.05$). These peaks occurred around 200–300 ms after stimulus onset, suggesting that categorical representations begin to emerge in the inferior temporal cortex during this time window. However, the relatively weak overall correlation suggests that the population code in IT may encode more fine-grained stimulus features or identity rather than only category-level distinctions. This result also complements the modest classification and mutual information results observed earlier, indicating that category-selective information may be present but not strongly separable across all stimuli or neurons.

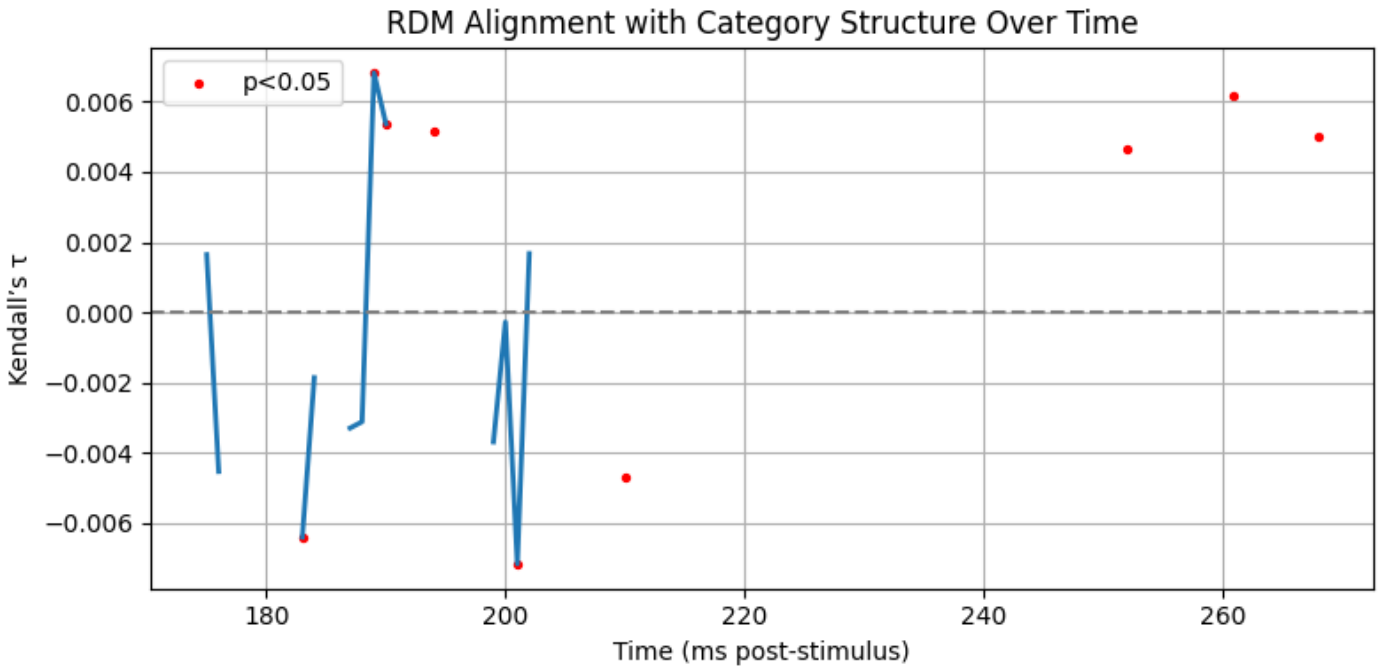


*Figure 34 - RDM and Kendall Tau correlation*

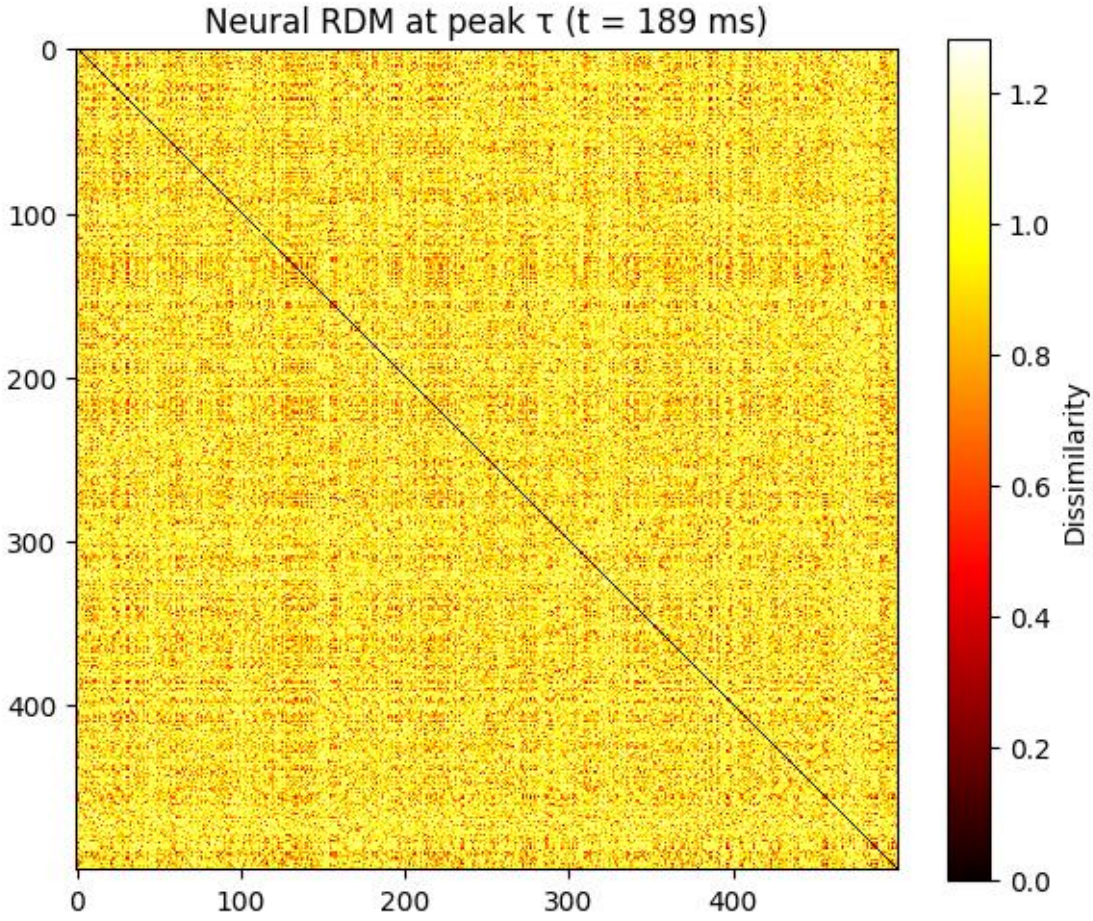


*Figure 35 - RDM at the peak*

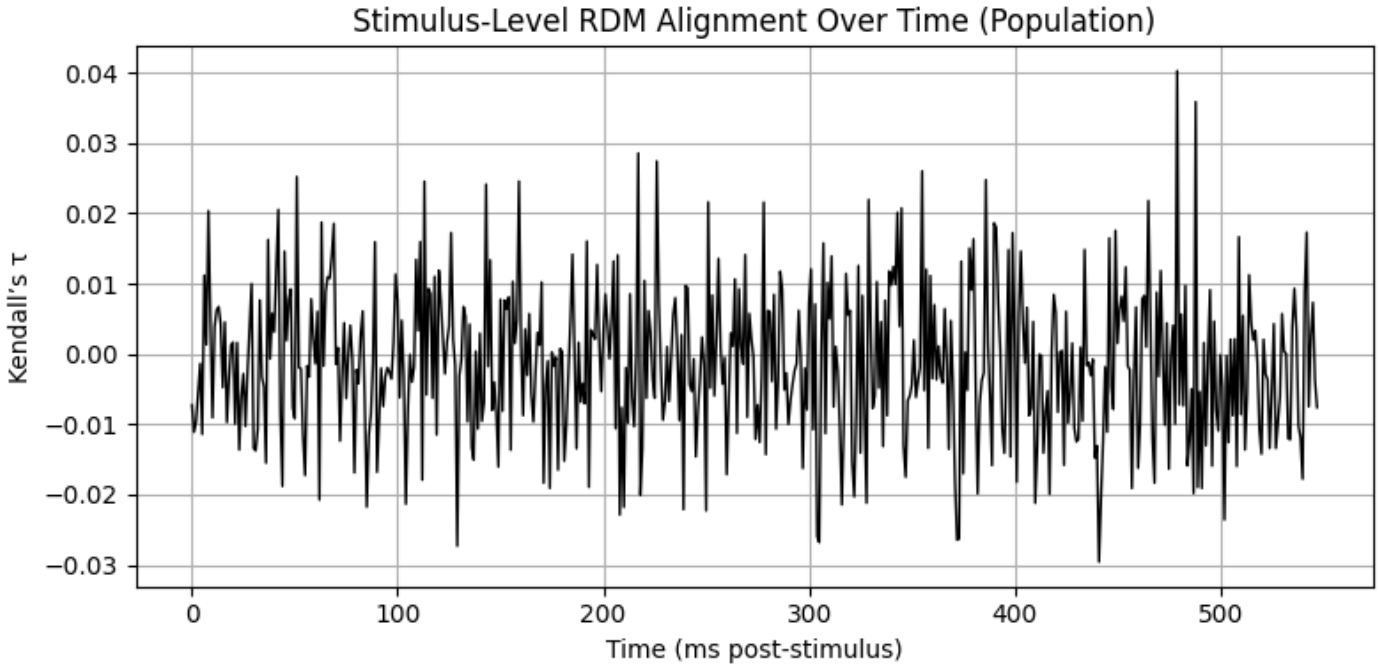


*Figure 36 - Stimulus level RDM*

In conclusion, the RDM and Kendall's tau analysis provided a time-resolved, model-independent view of how neural response patterns relate to semantic stimulus structure. While category information was reflected to some degree in the population response

geometry, it appeared in brief and specific time periods, consistent with the idea that categorical representations are transient and distributed across neurons. Further analysis focused on category-selective neurons or finer-grained category structure could provide a more detailed understanding of these dynamics.

## 4.2 Generalized Linear Model (GLM)

In this part of the project, we aimed to understand how well the firing activity of individual neurons could be predicted from the semantic category of the stimulus. To accomplish this, we employed a Generalized Linear Model (GLM) framework to regress each neuron's spike count against the stimulus category label. GLMs are a powerful and flexible statistical tool that allow for modeling relationships between a response variable (in this case, spike count) and one or more explanatory variables (in this case, stimulus category), even when the response distribution is non-Gaussian.

We first computed spike counts for each neuron in a post-stimulus window of interest, typically 100–300 ms, as this window has been shown in previous parts (e.g., PSTH and RDM analyses) to contain meaningful category-selective responses. These spike counts served as the dependent variable in the model. The independent variable was the category label of the presented stimulus (Face, Body, Natural, or Artificial), encoded as integers 0 through 3. We used a Poisson GLM, which is appropriate for modeling spike count data, as it captures both the discrete and non-negative nature of neural firing rates.

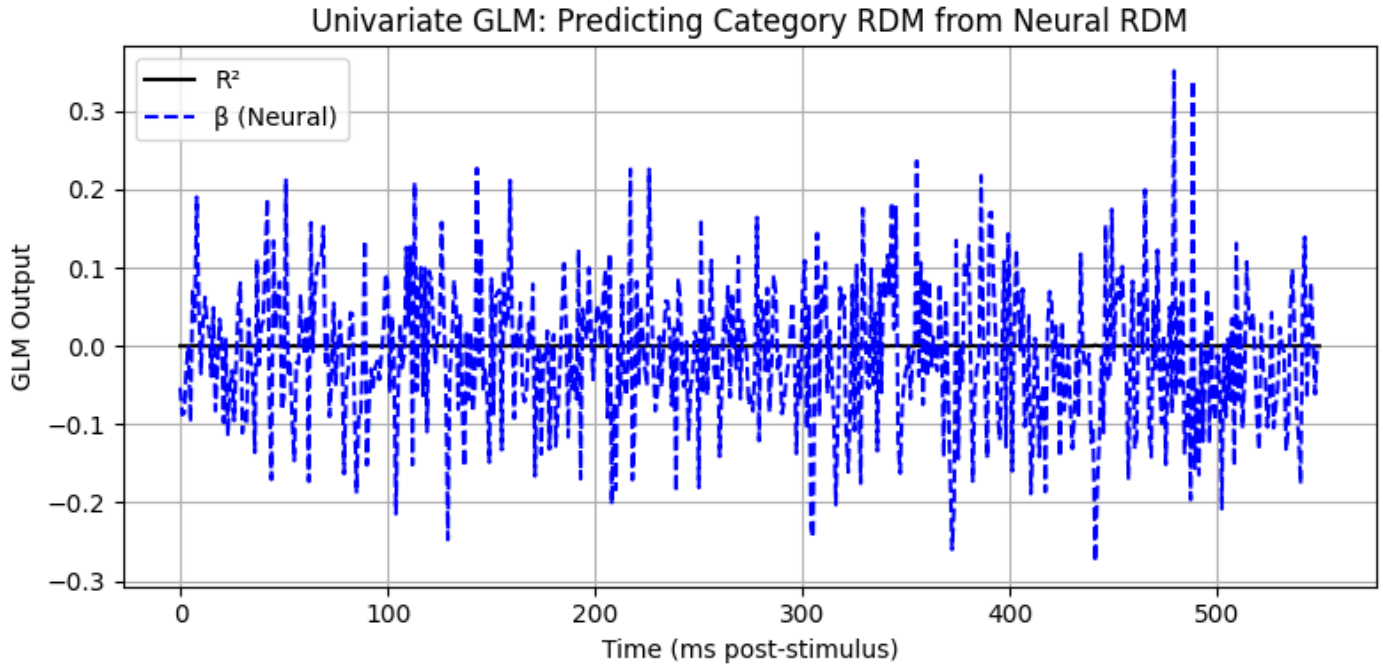


*Figure 37 - GLM for RDM*

For each neuron, we fit a separate GLM and evaluated the goodness of fit by examining the model's deviance explained. Neurons with higher deviance explained values indicate stronger tuning to stimulus category, while those with near-zero values suggest little or no category selectivity. The overall results showed that only a small subset of neurons were

well-explained by the GLM model, with most showing weak category-dependent modulation of firing rate. This was consistent with other analyses such as the Fano factor and mutual information, where category selectivity was modest and varied across the population.

In conclusion, the GLM analysis provided a model-based assessment of each neuron's categorical tuning. While most neurons did not strongly differentiate between stimulus categories at the firing rate level, the approach confirmed that a subset of the population does show significant category-selective modulation. These neurons may play a more prominent role in encoding semantic distinctions in the inferior temporal cortex and could be targeted in future decoding or representational analyses.